This article has been accepted for publication in a future issue of this journal, but has not been fully edited. Content may change prior to final publication. Citation information: DOI 10.1109/TIFS.2016.2541345, IEEE Transactions on Information Forensics and Security

Minutiae Extraction from Level 1 Features of Fingerprint

Eryun Liu, *Member, IEEE*, Kai Cao

***Abstract*—Fingerprint features can be divided into three major categories based on the granularity at which they are extracted: level 1, level 2 and level 3 features. Orientation field, ridge frequency field and minutiae set are three fundamental components of fingerprint, where the orientation field and ridge frequency field are regarded as level 1 features and minutiae set as level 2 features. It is generally believed that level 1 features, especially orientation field, can be reconstructed from level 2 features, i.e., minutiae. However, it is still a question that if minutiae can be extracted from level 1 features. In this paper, we analyze the relations between level 1 and level 2 features using the FM model and propose an approach to extract minutiae from level 1 features (i.e., orientation field and frequency field). The proposed algorithm is evaluated on NIST SD27 and FVC2002 DB1 databases. The true detection rate (TDR) and false detection rate (FDR) of minutiae detection on NIST SD27 and FVC2002 DB1 are about 45% and 30% compared to manually marked minutiae, respectively, with level 1 features extracted at a block size of 16 pixels. When pixel-wise orientation and frequency fields are available, TDR and FDR can reach 70% and 25%, respectively. With a smaller block size, the minutiae recovering accuracy can be even higher. Our quantitative and experimental results show the deep relationship between level 1 and level 2 features of a fingerprint.**

***Index Terms*—Fingerprint reconstruction, orientation field, ridge frequency field, minutiae, FM model**

I. Introduction

A fingerprint is the ridge friction pattern on a fingertip. Due to fingerprint's high discriminability and persistence over time, fingerprint-based person recognition systems have been widely deployed. It is generally agreed that fingerprint recognition systems have played a crucial role in various applications, including law enforcement, forensics, physical and logical access control, border crossing and civil registry.

Orientation field, ridge frequency field and minutiae set are three fundamental components that constitute a fingerprint image. Fingerprint features can be divided into three major categories based on the granularity at which they are extracted: level 1, level 2 and level 3 features. The orientation field and ridge frequency field are regarded as level 1 features and minutiae set as level 2 features. In [1], the author proposed a FM model that combines both level 1 and level 2 features under a unified framework.

It is generally believed that level 1 features, especially orientation field, can be reconstructed from level 2 features, i.e., minutiae. Hence the corresponding fingerprint image can be further reconstructed [3],[4],[5],[6],[7],[8]. However, it is still a question that if minutiae can be inferred from level 1 features. Minutiae are generally considered as a type of higher level of fingerprint features because it contains both locations and directions of feature points. In this paper, we are interested in the relationship between level 1 and level 2 features of a fingerprint and how well the level 2 features (i.e., minutiae) can be inferred from level 1 features.

Various features in a fingerprint image are not independent of each other. These dependencies are not well studied in the literatures. We observed that the locations of minutiae in a fingerprint are highly related to its level 1 features. Fig. 1 illustrates this relationship between level 1 features and level 2 features. Even though the central part of a portion of fingerprint images are covered by a white box, we can still guess whether there is a minutia within the box or not. In Fig. 1(a), there are four ridges (in white color) emanating from the left side of box, but five ridges coming out from the right side of the box. So, we can guess there is a minutia with direction pointing to the right side in the white box. On the other hand, in Fig. 1(b), the ridges are going through the white box in an opposite way and we can infer there is a minutia in the white box with direction pointing to the left side. In Fig. 1(c), there are four ridges coming in from the left side and four ridges coming out from the right side. This enables us to infer that there may be either no minutia within the white box or there may be two minutiae with opposite directions.

In this paper, we study the theoretical relationship between level 1 and level 2 features and show that the minutiae features can also be inferred from level 1 features of a fingerprint. According to the FM model [1], an ideal fingerprint F can be represented as $F = \cos(\Phi) = \cos(C + S)$, where C is the continuous phase image without any global spirals, S is the spiral phase image constructed by minutiae, and Φ is a composite phase that can be uniquely decomposed into C and S according to the Helmholtz Decomposition Theorem [10]. The ridge orientation of fingerprint F is perpendicular to the angle of gradient field of composite phase Φ, and the ridge frequency is the magnitude of local instantaneous frequency. With given orientation field and ridge frequency field (level 1 features) as inputs, we propose to use curve integral on the

Eryun Liu is with the Zhejiang Provincial Key Laboratory of Information Network Technology, College of Information Science & Electronic Engineering, Zhejiang University, Hangzhou, Zhejiang 310027, China.
E-mail: eryunliu@zju.edu.cn

Kai Cao is with the Dept. of Computer Science and Engineering, Michigan State University, East Lansing, MI 48824 U.S.A.
E-mail: kaicao@cse.msu.edu

This article has been accepted for publication in a future issue of this journal, but has not been fully edited. Content may change prior to final publication. Citation information: DOI 10.1109/TIFS.2016.2541345, IEEE Transactions on Information Forensics and Security

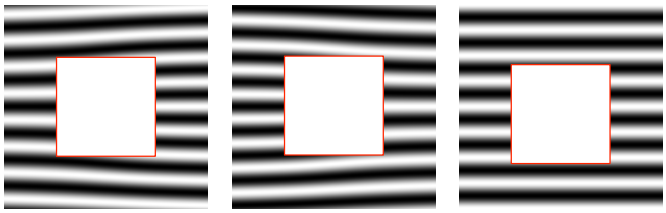

Fig. 1. Illustration of relationship between level 1 and level 2 features. Only small portions of fingerprints are shown here. Examples of ridge pattern where (a) there is a minutia whose direction is pointing to the right in the white box; (b) there is a minutia whose direction is pointing to the left in the white box; (c) there may be no minutia in the white box or two minutiae with opposite directions.

gradient field of composite phase to first detect the minutiae location map. Each minutia appears as a blob like feature in the minutiae location map. Then, a blob feature detector, SURF keypoint detector [11], is applied on the minutiae location map to localize the blobs. After a series of post processing operations on the detected blobs, minutiae features can be successfully recovered. With the detected minutiae, and the given orientation field and ridge frequency field, we also show that the fingerprint image can be further reconstructed by applying the FM model based fingerprint reconstruction algorithm proposed in [5] (see Fig. 5). Our study reveals the deep relation between level 1 and level 2 features and is helpful in better understanding the nature of fingerprint model and relations among feature components.

The rest of this paper is organized as follows. In section II, the relationship between level 1 and level 2 features and the detailed implementation of the proposed fingerprint reconstruction algorithm are presented. Experimental results are described and discussed in section IV and the conclusions are drawn in section V.

II. Relationship between Level 1 and Level 2 Features

A. Fingerprint Representation

According to the FM model [1], an ideal fingerprint $I(x,y)$ can be represented as [1]

$$I(x,y) = \cos\left(\Phi(x,y)\right). \tag{1}$$

According to the Helmholtz Decomposition Theorem [10], the phase $\Phi(x,y)$ can be uniquely decomposed into a continuous phase $C(x,y)$ and a spiral phase $S(x,y)$

$$\Phi(x,y) = C(x,y) + S(x,y). \tag{2}$$

Thus, phase $\Phi(x,y)$ is also termed as composite phase. Fig. 2 shows an example of a fingerprint with its continuous phase and spiral phase. While the continuous phase image is smooth and changes slightly, the spiral phase image contains many singular points that appear at the locations of minutiae points.

[1]The level 3 fingerprint features are not considered in the FM model.

B. Orientation field and ridge frequency field

The gradient field (I_x, I_y) of fingerprint image $I(x,y)$ is

$$I_x = -\sin\left(\Phi(x,y)\right)\frac{\partial\Phi(x,y)}{\partial x} = -\sin\left(\Phi(x,y)\right)\omega_x, \tag{3}$$

$$I_y = -\sin\left(\Phi(x,y)\right)\frac{\partial\Phi(x,y)}{\partial y} = -\sin\left(\Phi(x,y)\right)\omega_y. \tag{4}$$

The orientation field $o(x,y)$ can be computed as

$$o(x,y) = \arctan\left(\frac{I_x}{I_y}\right) = \arctan\left(\frac{\omega_x}{\omega_y}\right). \tag{5}$$

Thus, the gradient field (ω_x, ω_y) of composite phase $\Phi(x,y)$ can uniquely determine the orientation field $o(x,y)$. It should be noted that the ridge orientation is in range $[-\frac{\pi}{2}, \frac{\pi}{2})$, or the wrapped direction plus $\frac{\pi}{2}$ of gradient field (ω_x, ω_y).

The local ridge frequency of fingerprint is simply the amplitude of gradient field of composite phase $\Phi(x,y)$. That is $\sqrt{\omega_x^2 + \omega_y^2}$.

C. Curve Integral on Gradient Field of $\Phi(x,y)$

Now, we consider the curve integral on gradient field (ω_x, ω_y) along a closed path l

$$\begin{aligned} P &= \oint_l (\omega_x, \omega_y)\mathrm{d}\vec{l} = \oint_l \nabla\Phi(x,y)\mathrm{d}\vec{l} && (6)\\ &= \oint_l \left(\nabla C(x,y) + \nabla S(x,y)\right)\mathrm{d}\vec{l} && (7)\\ &= \oint_l \nabla C(x,y)\mathrm{d}\vec{l} + \oint_l \nabla S(x,y)\mathrm{d}\vec{l}, && (8)\end{aligned}$$

where ∇ is the gradient operator. Since the continuous phase $C(x,y)$ is a smooth function (or with 2π difference) according to Helmholtz Decomposition Theorem (see Fig. 2(b)), we have

$$\oint_l \nabla C(x,y)\mathrm{d}\vec{l} = 0. \tag{9}$$

The spiral phase $S(x,y)$ can be represented by minutiae set as

$$S(x,y) = \sum_{i=1}^{N} p_i \arctan\left(\frac{y-y_i}{x-x_i}\right), \tag{10}$$

where N is the number of minutiae in the fingerprint I and $p_i \in \{1,-1\}$ denotes the polarity of the minutia at (x_i, y_i). So,

$$\begin{aligned} \oint_l \nabla S(x,y)\mathrm{d}\vec{l} &= \oint_l \nabla \sum_{i=1}^{N} p_i \arctan\left(\frac{y-y_i}{x-x_i}\right)\mathrm{d}\vec{l} && (11)\\ &= \sum_{i=1}^{N} p_i \oint_l \nabla \arctan\left(\frac{y-y_i}{x-x_i}\right)\mathrm{d}\vec{l}. && (12)\end{aligned}$$

When the minutia (x_i, y_i) is outside of the closed path l, the integral

$$\oint_l \nabla \arctan\left(\frac{y-y_i}{x-x_i}\right)\mathrm{d}\vec{l} = 0. \tag{13}$$

Thus, the overall integral $P = \oint_l \nabla\Phi(x,y)\mathrm{d}\vec{l} = 0$, if all the minutiae are outside of the closed path l.

This article has been accepted for publication in a future issue of this journal, but has not been fully edited. Content may change prior to final publication. Citation information: DOI 10.1109/TIFS.2016.2541345, IEEE Transactions on Information Forensics and Security

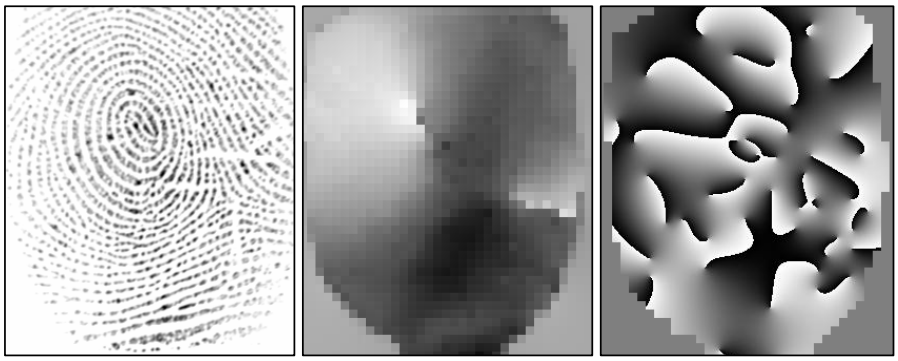

Fig. 2. An example of a fingerprint and its phase images; (a) a plain fingerprint in FVC2002 DB1 [2]; (b) continuous phase $C(x,y)$, and (c) spiral phase $S(x,y)$ of fingerprint image shown in (a).

Otherwise, let $F=(S_x,S_y)=\nabla S_{ij}(x,y)$ be the gradient field of spiral phase $S_{ij}(x,y)=\arctan\left(\frac{y-y_i}{x-x_i}\right)$ of minutia at (x_i,y_i), we have

$$S_x = \frac{\partial S_{ij}}{\partial x}=\frac{-(y-y_i)}{(x-x_i)^2+(y-y_i)^2}, \quad (14)$$

$$S_y = \frac{\partial S_{ij}}{\partial y}=\frac{(x-x_i)}{(x-x_i)^2+(y-y_i)^2}. \quad (15)$$

Then,

$$\oint_l S_{ij}(x,y)\mathrm{d}\vec{l} = \oint_l \nabla \arctan\left(\frac{y-y_i}{x-x_i}\right)\mathrm{d}\vec{l} \quad (16)$$

$$= \oint_l (S_x,S_y)\mathrm{d}\vec{l} \quad (17)$$

$$= 2\pi. \quad (18)$$

With Eqs. (9), (12) and (18), we have the overall integral

$$P=\oint_l \nabla\Phi(x,y)\mathrm{d}\vec{l}=\oint_l \nabla S(x,y)\mathrm{d}\vec{l}=2\pi\sum_{k\in\mu}p_k, \quad (19)$$

where μ is the set of index numbers of minutiae which are located within the closed path l.

When there is only one minutia, say (x_i,y_i), within l, we have

$$P=\oint_l \nabla\Phi(x,y)\mathrm{d}\vec{l}=2\pi p_i. \quad (20)$$

The curve integral along a closed path is essentially computing the phase change along this path. Since a spiral phase adds or reduces one period of phase (i.e., 2π) on the composite phase $\Phi(x,y)$, an additional ridge will appear or disappear around this minutia. However, from the curve integral value, we cannot infer the exact number of minutiae because the minutiae of different polarities within closed path l will cancel each other in Eq. (19) . This explains the phenomenon shown in Fig. 1.

D. Minutiae Direction

The minutiae direction is determined by the direction of phase gradient and minutiae polarity. In [5], the authors demonstrated the relationship between minutiae direction and polarity. Here, we further investigate how the local phase gradient of continuous phase affects the minutiae direction. Fig. 3 shows some examples of synthetic local ridge patterns with different combinations of local phase gradient and minutiae polarity.

The relationship among minutiae direction, minutiae polarity and the angle of local phase gradient can be derived from these examples

$$\beta=\theta-\frac{p\pi}{2}, \quad (21)$$

where β is the minutia direction, θ is the direction of phase gradient and $p\in\{-1,1\}$ is the minutia polarity. The direction of phase gradient θ can be estimated by orientation field $o\in[-\frac{\pi}{2},\frac{\pi}{2})$: $\theta=o\pm\frac{\pi}{2}$. Without any loss of generality, we use $\theta=o-\frac{\pi}{2}$.

Fig. 4 shows some examples of curve integral values in different synthetic local regions of ridge patterns.

III. Implementation of Minutiae Inference

The flowchart of the proposed fingerprint reconstruction algorithm from given orientation field and ridge frequency field is shown in Fig. 5. Based on the theoretical analysis in the previous section, we discretize the curve integral of Eq. (19) for recovering minutiae from the given orientation field and ridge frequency field. Since the curve integral value is independent of the shape of the closed path l, we use a circle of radius R as the integral path for simplicity.

A. Minutiae Location Map

The circle l is uniformly divided into K segments in clockwise direction, with each segment of length around $\frac{|l|}{K}$ pixels, where $|l|=2\pi R$ is the total length of l. Let $\{(u_i,v_i)|i=1,\cdots,K+1\}$ be the $K+1$ points used to divide l, where (u_1,v_1) is the starting point of l and (u_{K+1},v_{K+1}) is the ending point of l [2].

In Eq. (6), the circle integral can be approximated as

$$\oint_l \nabla\Phi(x,y)\mathrm{d}\vec{l} \approx \sum_{i=1}^{K}\vec{\omega}^{(i)}\cdot\triangle\vec{l}^{(i)}, \quad (22)$$

[2]Note that (u_{K+1},v_{K+1}) is the same as (u_1,v_1) for a closed path. So, there are actually only K points dividing the circle.

This article has been accepted for publication in a future issue of this journal, but has not been fully edited. Content may change prior to final publication. Citation information: DOI 10.1109/TIFS.2016.2541345, IEEE Transactions on Information Forensics and Security

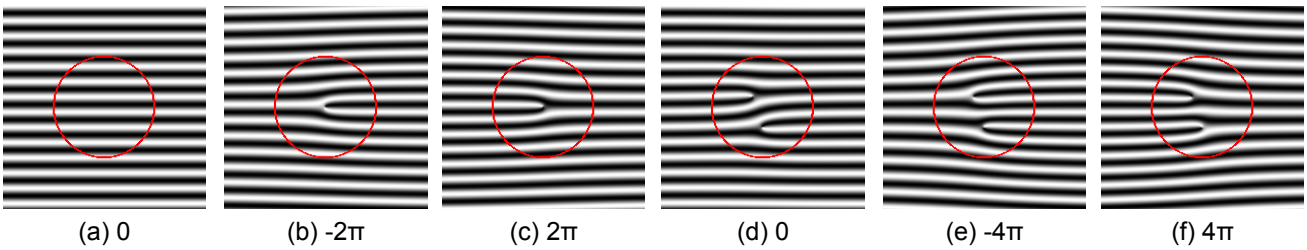

Fig. 4. Examples of curve integral in different synthetically generated local regions of ridge patterns. Red circles indicate the closed integral path.

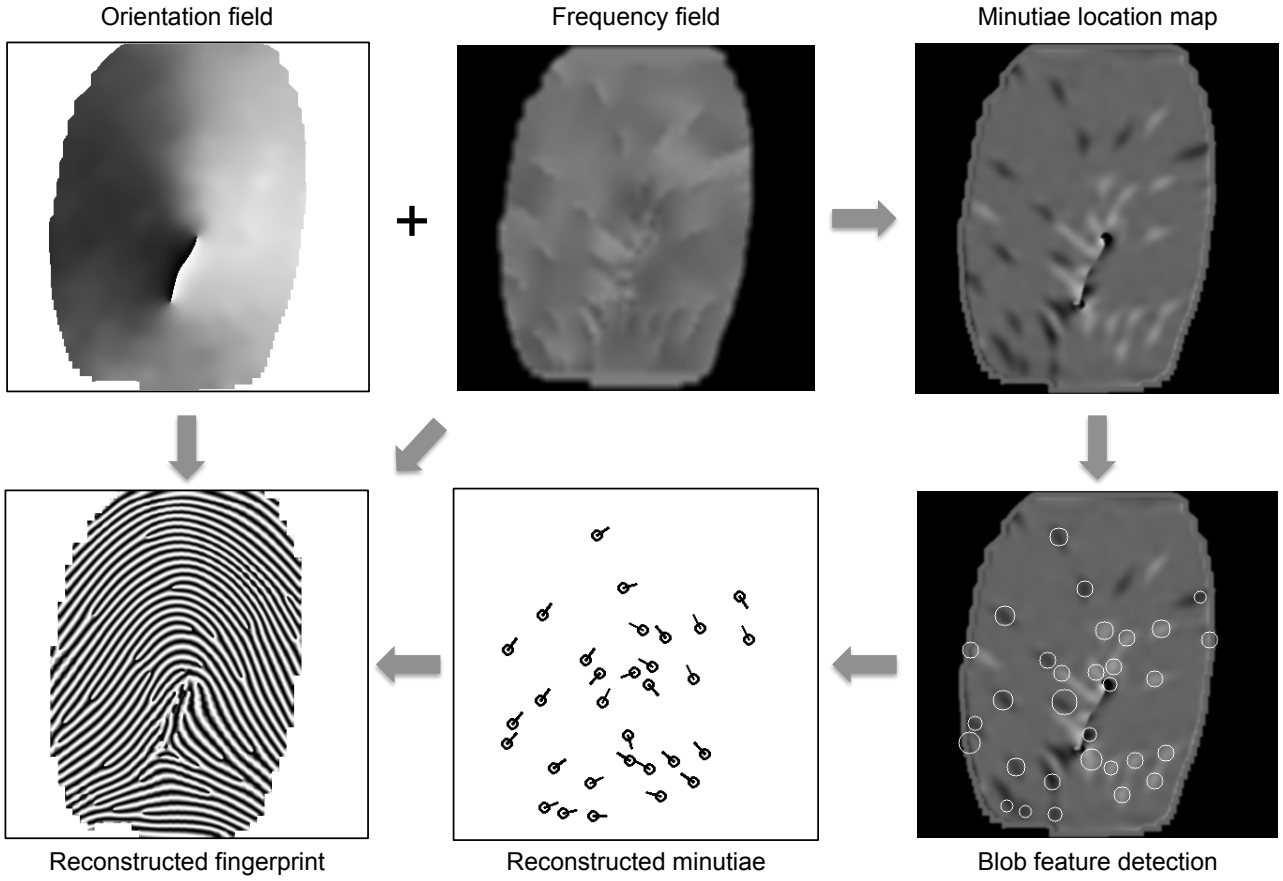

Fig. 5. Flowchart of the proposed fingerprint reconstruction algorithm from given orientation field and ridge frequency field.

where $\vec{\omega}^{(i)}$ is the instantaneous frequency (or gradient vector) of composite phase Φ at the center of the ith segment on circle l; it can be estimated as

$$\vec{\omega}^{(i)} = |\vec{\omega}^{(i)}|(\sin\theta^{(i)}, \cos\theta^{(i)}), \tag{23}$$

where $|\vec{\omega}^{(i)}|$ is the magnitude of vector $\vec{\omega}^{(i)}$ and $\theta^{(i)}$ is the angle of gradient vector $\vec{\omega}^{(i)}$. Although the gradient vector, $\vec{\omega}^{(i)}$, is normal to the local ridge orientation field, we cannot simply add or subtract $\frac{\pi}{2}$ to the ridge orientation to obtain the angle of gradient vector because the ridge orientation is wrapped to range $[-\frac{\pi}{2}, \frac{\pi}{2})$. To resolve the ambiguity, we need to unwrap the orientation field so as to obtain the angle of gradient vector. Without lack of generality, we set the angle $\theta^{(0)}$ of gradient vector at the center point of circle l as the ridge orientation minus $\frac{\pi}{2}$ (i.e., $o^{(0)} - \frac{\pi}{2}$). For each segment on l, its initial angle $\theta^{(i)}$ of gradient vector is set to $(o^{(i)} - \frac{\pi}{2})$. Then, the unwrapped angle of phase gradient of each segment can be determined from the initial angle recursively as

$$\theta^{(i)} = \begin{cases} \theta^{(i)} - \pi, & \text{if } \theta^{(i)} - \theta^{(i-1)} > \frac{\pi}{2}, \\ \theta^{(i)} + \pi, & \text{if } \theta^{(i-1)} - \theta^{(i)} > \frac{\pi}{2}, \\ \theta^{(i)}, & \text{otherwise.} \end{cases} \tag{24}$$

The vector $\triangle\vec{l}^{(i)}$ in Eq. (22) is the vector of the ith line segment from (u_i, v_i) to (u_{i+1}, v_{i+1}) and can be represented as

$$\triangle\vec{l}^{(i)} = (u_{i+1} - u_i, v_{i+1} - v_i) \tag{25}$$

$$= \frac{|l|}{K}(\sin\alpha^{(i)}, \cos\alpha^{(i)}), \tag{26}$$

where $\alpha^{(i)}$ is the angle of vector $\triangle\vec{l}^{(i)}$. Suppose the center point $(\frac{u_1+u_2}{2}, \frac{v_1+v_2}{2})$ of the first line segment is on the right

This article has been accepted for publication in a future issue of this journal, but has not been fully edited. Content may change prior to final publication. Citation information: DOI 10.1109/TIFS.2016.2541345, IEEE Transactions on Information Forensics and Security

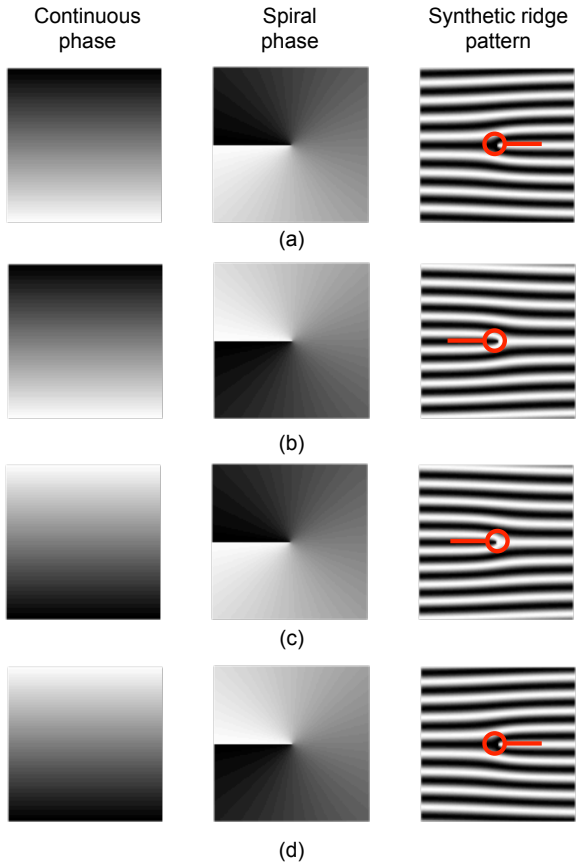

Fig. 3. Illustration of the relationships among minutiae direction, phase gradient and minutiae polarity.

side of circle l and $\frac{v_1+v_2}{2} = y_c$, where (x_c, y_c) is the center of circle l, the angle $\alpha^{(i)}$ can be obtained by

$$\alpha^{(i)} = (i-1)\frac{2\pi}{K} + \frac{\pi}{2}, i = 1, 2, \cdots, K. \tag{27}$$

So, Eq. (22) can be rewritten as

$$\begin{aligned} P &= \oint_l \nabla\Phi(x,y)\mathrm{d}\vec{l} \\ &\approx \sum_{i=1}^{K} |\omega^{(i)}|(\sin\theta^{(i)}, \cos\theta^{(i)}) \cdot \frac{|l|}{K}(\sin\alpha^{(i)}, \cos\alpha^{(i)}) \\ &= \frac{|l|}{K}\sum_{i=1}^{K} |\omega^{(i)}| \cos\left(\theta^{(i)} - \alpha^{(i)}\right) \qquad (28) \\ &= \frac{2\pi|l|}{K}\sum_{i=1}^{K} f^{(i)} \cos\left(\theta^{(i)} - \alpha^{(i)}\right), \qquad (29) \end{aligned}$$

where $f^{(i)} = \frac{\omega^{(i)}}{2\pi}$ is the ridge frequency at the center of the ith line segment on l.

For each pixel in the fingerprint image, we perform a curve integral to obtain a minutiae location map value P. A Gaussian filter of size 7×7 with $\sigma = 1$ is then applied to P. On the minutiae location map P, a large absolute value of integral value denotes a high possibility there is a minutia.

It should be noted that the radius R of circle l has an effect on the minutiae location map (see Fig. 6). A smaller circle can provide a more accurate estimation of minutiae location, but requires a more accurate orientation field and ridge frequency field; on the other hand, a large circle may miss some minutiae when the minutiae are very close to each other. In general, the radius can be set to around local ridge period. In this paper, we set the radius R to different values depending on the inputs. If both orientation field and ridge frequency field are available, the radius R is set to 8 pixels. When only the orientation field is available, the radius R is set to 10 pixels for robustness.

B. Minutiae Localization

As we analyzed previously, the curve integral value is $\pm 2\pi$ around a closed path enclosing a minutia. Since we use a circle of radius R as the integral path, ideally there is a sharp white ($+2\pi$) or black (-2π) circular spot (or blob) around each minutia on the minutiae location map, with the rest of region being 0. However, due to the present of noise, the spots boundaries are blurred (see Fig. 7(a)).

SIFT is a classic scale invariant keypoint detector and feature descriptor which detects scale-space local extrema [9]. Each extrema point represents the center of blob in image. This property is very suitable for our task of detecting minutiae in minutiae location map.

We adopt the SURF keypoint detector [3] (a speed-up version of SIFT) proposed in [11] to detect the blob features in $|P|$, where $|P|$ is the absolute value of P. Let $B = \{(x_i, y_i, s_i)\}$ be the set of detected blobs, where x_i and y_i are the blob coordinates, and s_i is the scale of the blob. A large scale value s_i corresponds to a large blob size. In the initially detected blob set B, there are many falsely detected minutiae (see Fig. 7(b)). A set of additional constraints is applied on B for refining the blob features so as to recover the minutiae set:

1) The absolute value of curve integral $P(x_i, y_i)$ at (x_i, y_i) should be greater than a threshold value T_P.
2) The scale s_i of each blob should be within the range $[s_{min}, s_{max}]$.
3) If the distance dis_{ij} between two blobs is less than a threshold T_{dis}, then remove both blobs.
4) If the $(s_i + s_j - dis_{ij}) > T_s$, where T_s is a predefined threshold, then keep the blob with smaller scale.

After applying the above conditions, many falsely detected blobs are removed, and the locations of final minutiae are determined as the blob locations. Let $\{(x'_i, y'_i, \beta_i)\}$ be the set of detected minutiae. According to Eq. (21), the minutia direction β_i can be determined as

$$\beta_i = \begin{cases} o(x'_i, y'_i), & \text{if } P(x'_i, y'_i) < 0, \\ o(x'_i, y'_i) - \pi, & \text{otherwise}, \end{cases} \tag{30}$$

where $o(x'_i, y'_i)$ is the ridge orientation field at (x'_i, y'_i). Fig. 7(c) shows the refined blob features in minutiae location map, and Fig. 7(d) shows the detected minutiae in the skeleton image.

[3] In this paper, the implementation of SURF detector in OpenCV library [13] is used to detect blobs.

This article has been accepted for publication in a future issue of this journal, but has not been fully edited. Content may change prior to final publication. Citation information: DOI 10.1109/TIFS.2016.2541345, IEEE Transactions on Information Forensics and Security

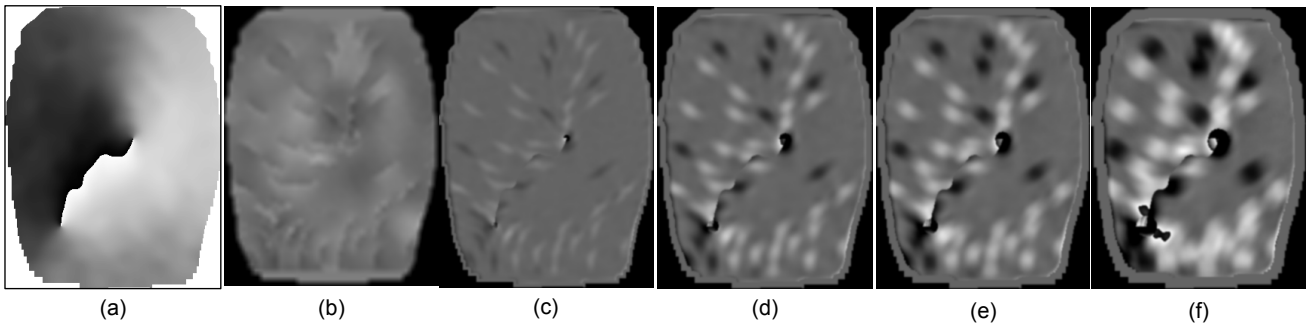

Fig. 6. Illustration of minutiae location map obtained with different areas of circle integral; (a) orientation field; (b) ridge frequency field; (c) $R = 2$; (d) $R = 6$; (e) $R = 10$; (f) $R = 14$. The unit of radii is in pixels and the level 1 features shown in (a) and (b) are extracted in pixel-wise.

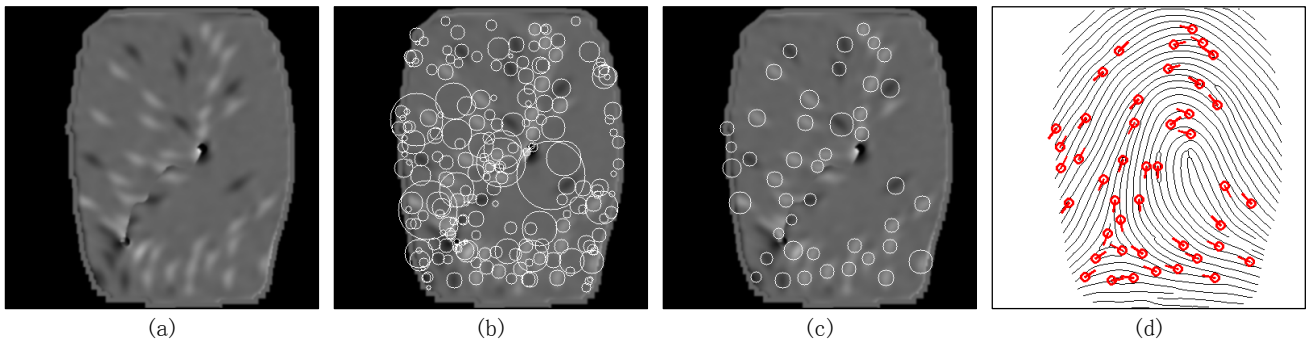

Fig. 7. Illustration of minutiae localization by blob feature detection and refinement. (a) Minutiae location map; (b) initial detected blobs shown as circles; (c) refined blobs; (d) detected minutiae overlaid on the skeleton image.

IV. Experimental Results

A. Databases

The proposed minutiae recovering algorithm is evaluated on FVC2002 DB1, FVC2002 DB2 [17] and NIST SD27 [12] databases. In FVC2002 DB1 and NIST SD27, the manually marked minutiae are available as ground truth for comparison purpose [16].

B. Minutiae Detection Accuracy

In an operational fingerprint recognition system, the level 1 features may be computed in block-wise manner as opposed to pixel-wise manner. For example, in [15], the orientation field and ridge frequency are estimated for every non-overlapping block of size 16×16 pixels. To investigate how the minutiae detection accuracy is affected by block size, we compute the orientation field and ridge frequency at different block sizes.

A manually marked minutia $m(x, y, \beta)$ is deemed as detected correctly if there is a minutia $m'(x', y', \beta')$ in the extracted minutiae set that satisfies the following two conditions:

$$\sqrt{(x - x')^2 + (y - y')^2} < d, \tag{31}$$

$$\phi(\beta, \beta') < \Delta\beta, \tag{32}$$

where d and $\Delta\beta$ are two thresholds set to 20 pixels and 20 degree, respectively; $\phi(\beta, \beta')$ denotes the minimum angle that rotates β to β', either clockwise or counter-clockwise.

Two measures are used to evaluate the minutiae detection accuracy. The first measure is called the *False Detection Rate* (FDR), which is defined as

$$\text{FDR} = \frac{\text{Number of falsely detected minutiae}}{\text{Total number of detected minutiae}}. \tag{33}$$

The second measure is called the *True Detection Rate* (TDR), which is defined as

$$\text{TDR} = \frac{\text{Number of truly restored minutiae}}{\text{Total number of ground truth minutiae}}. \tag{34}$$

On NIST SD27 rolled fingerprints, only the minutiae above the first knuckle were marked, however, the proposed algorithm detects minutiae on the whole image. To reduce the side effect of region below the first knuckle, we only use the extracted minutiae within the convex hull of manually marked minutiae for measuring minutiae detection accuracy on the NIST SD27 rolled print database.

Fig. 8 shows the FDR and TDR for FVC2002 DB1 and NIST SD27 (rolled and latent) databases under different block sizes. Figs. 8 (a) and (b) are FDR and TDR using both orientation and ridge frequency field, while in Figs. 8 (c) and (d) only orientation fields were used in minutiae detection and the ridge frequency was fixed to a constant number (i.e., 0.125 in this experiment). The results show that when pixel-wise orientation and ridge frequency fields were used, we can have about a TDR of 70% at a FDR of about 25%. As we increase the block size, as expected, the TDR decreases accordingly; FDR is stable initially (or decreases slightly) and then increases rapidly when block size is greater than 16 pixels. In Figs. 8 (c) and (d), we observe a similar trend in TDR and FDR with increasing block size. However, as

This article has been accepted for publication in a future issue of this journal, but has not been fully edited. Content may change prior to final publication. Citation information: DOI 10.1109/TIFS.2016.2541345, IEEE Transactions on Information Forensics and Security

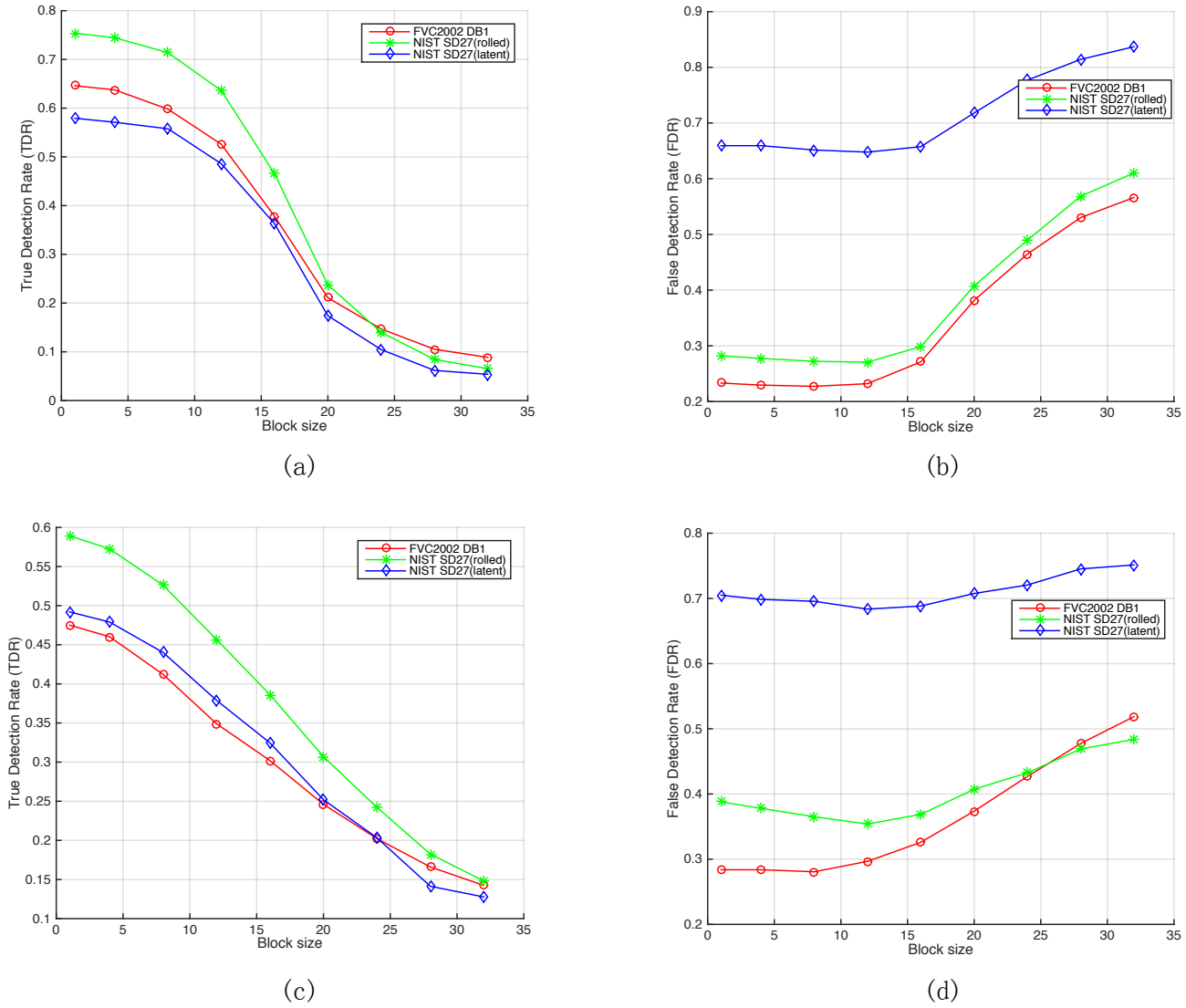

Fig. 8. Minutiae detection accuracy for different block sizes; (a) and (b) true detection rate and false detection rate, respectively, using reconstruction images from orientation field and ridge frequency field; (c) and (d) true detection rate and false detection rate, respectively, using reconstructed images from orientation field alone.

expected, the minutiae detection accuracy based on orientation field alone is much lower than that based on both orientation and ridge frequency fields.

From Fig. 8, we can also observe that the fingerprint image quality is a critical factor that affects the FDR. The FDRs on NIST SD27 latent prints are much higher than those on the other two datasets.

As a comparison with traditional minutiae detectors which detect minutiae from the original grayscale images, we compare the FDR and TDR of Verifinger SDK 6.5 [14] and the proposed algorithm on FVC2002 DB1 and NIST SD27 where the manually marked minutiae are available (see Table I). The results of block size 8 and 16 pixels of our algorithm are reported. It should be noted that we are not intent to improve the minutiae extraction accuracy over traditional ones. The main focus of this paper is to investigate the relationships between level 1 and level 2 features.

C. Matching Results

With the extracted minutiae, the fingerprint image can be reconstructed together with level 1 features by [5]. To further evaluate the accuracy of minutiae extraction, we conducted two types of matching experiments on FVC2002 DB1 and DB2 databases under the attack models in [5], where the type-I attack refers to matching the reconstructed fingerprint image against the original grayscale image and the type-II attack refers to matching the reconstructed fingerprint image against the grayscale image of the same finger but a different impression. The fingerprint image is reconstructed either from orientation and frequency fields (Ori + Fre) or from orientation field alone (Ori alone). The matching results under different block sizes are reported in Fig. 9, where TAR is true acceptance rate and FAR is false acceptance rate. We see that the TAR in Type-II attack is much higher than that in Type-I attack as expected, and combining orientation field and frequency

This article has been accepted for publication in a future issue of this journal, but has not been fully edited. Content may change prior to final publication. Citation information: DOI 10.1109/TIFS.2016.2541345, IEEE Transactions on Information Forensics and Security

TABLE I
COMPARISON OF MINUTIAE EXTRACTION ACCURACY (TDR AND FDR) OF PROPOSED METHOD AND VERIFINGER SDK 6.5 ON FVC2002 DB1 AND NIST SD27.

	FVC02 DB1		NIST27 Rolled		NIST27 Latent	
	TDR	FDR	TDR	FDR	TDR	FDR
Verifinger SDK	0.7928	0.0944	0.814	0.2393	0.663	0.6524
Proposed (Block size: 8)	0.5979	0.2273	0.7138	0.2722	0.5577	0.6516
Proposed (Block size: 16)	0.3781	0.2712	0.4653	0.2987	0.3628	0.6576

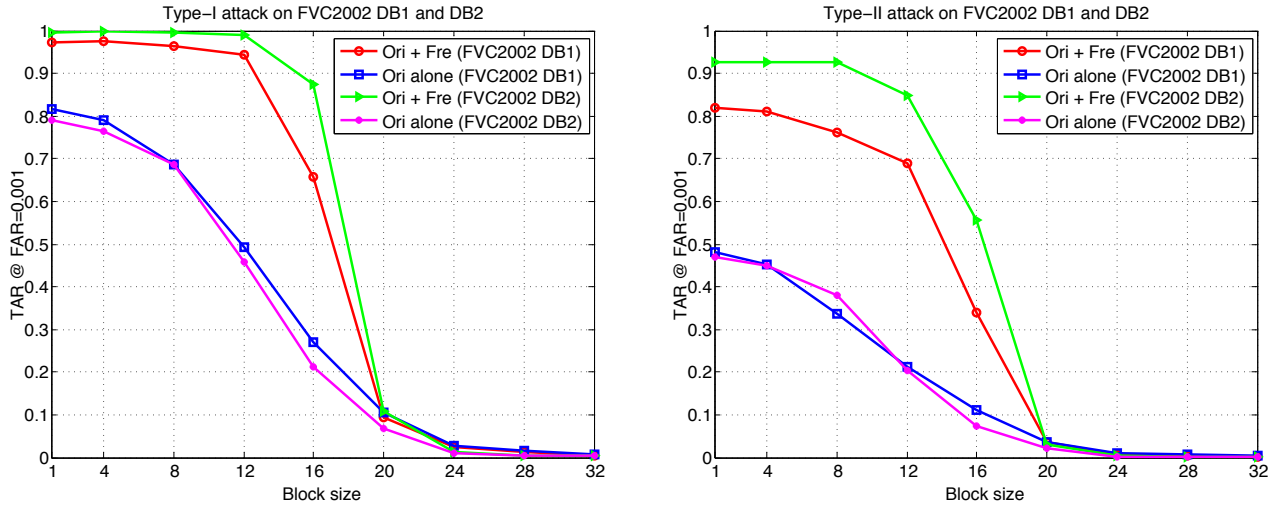

(a) (b)

Fig. 9. (a) Type-I and (b) Type-II attack on FVC2002 DB1 and DB2 databases.

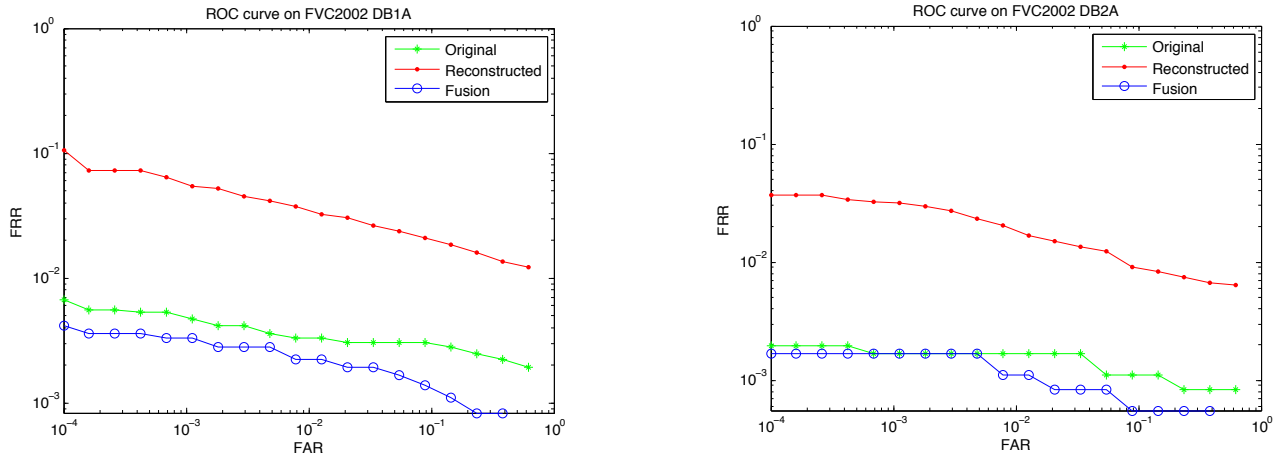

(a) (b)

Fig. 10. Fusion experiments on (a) FVC2002 DB1 and (b) FVC2002 DB2.

field is much better than orientation field alone. However, with orientation field alone, the TAR is still very high in Type-I attack when block size less than 20, indicating the high correlation between the extracted minutiae set from level 1 features and the original minutiae set.

To further investigate the feature correlations, we conduct fusion experiments on FVC2002 DB1 and DB2 databases with Verifinger matcher. In this experiment, we fuse the match scores, i.e., sum fusion, from original images and the reconstructed images together. The images are reconstructed from orientation and ridge frequency fields with block size of 4 pixels. Figure 10 shows the ROC curves. We see the performance of reconstructed image is inferior to that of original image. However, the fusion can help further improve the performance of using original image.

Fig. 11 compares the reconstructed fingerprint and minutiae

This article has been accepted for publication in a future issue of this journal, but has not been fully edited. Content may change prior to final publication. Citation information: DOI 10.1109/TIFS.2016.2541345, IEEE Transactions on Information Forensics and Security

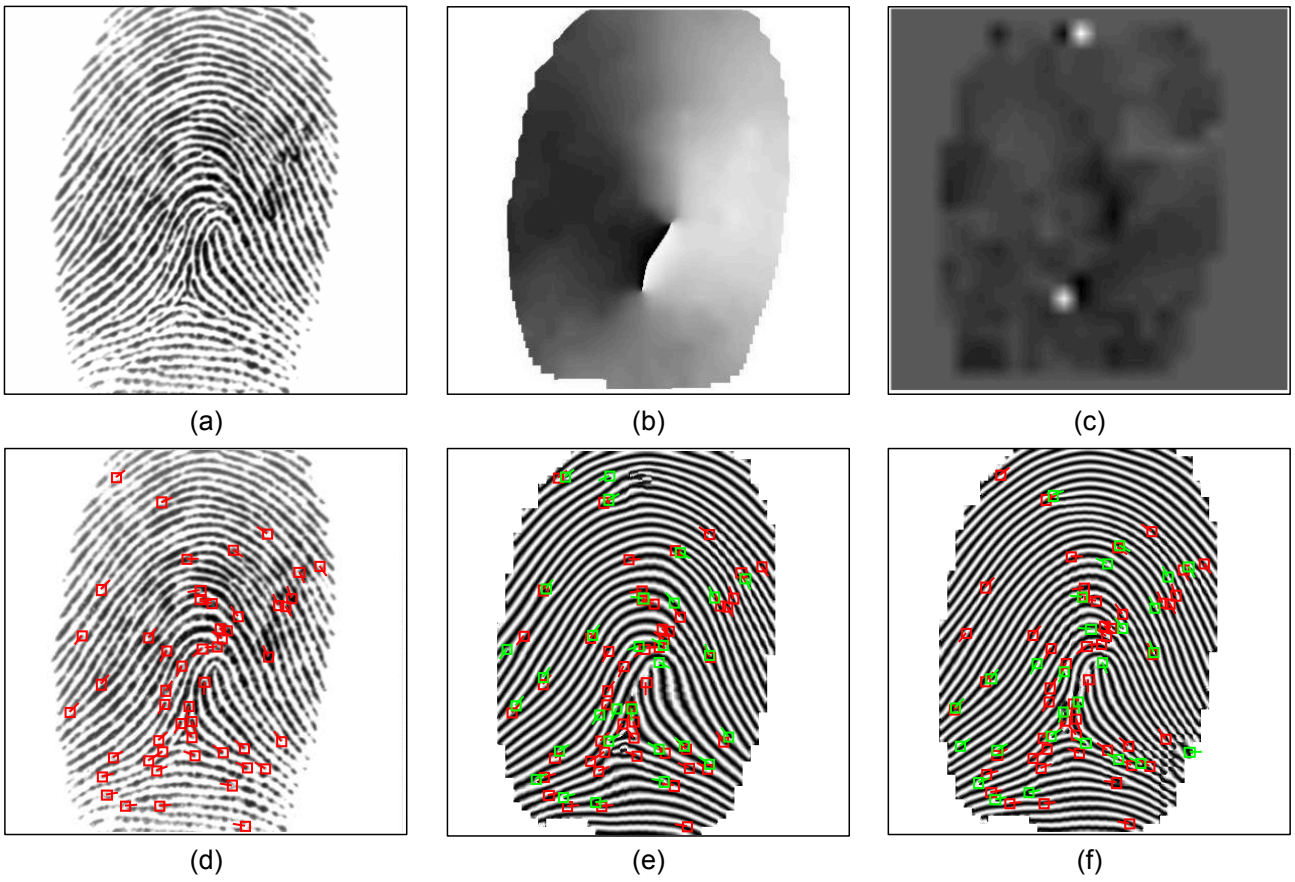

Fig. 11. An example showing (a) fingerprint image; (b) orientation field extracted from (a) with a block size of 16 pixels; (c) ridge frequency field extracted from (a) with a block size of 16 pixels; (d) manually marked minutiae (in red); (e) reconstructed minutiae (in green) and reconstructed fingerprint from (b) and (c) (FDR = 9.1% and TDR = 56.4%); and (f) reconstructed minutiae (in green) and reconstructed fingerprint from (b) alone (FDR = 30.4% and TDR = 43.6%). The red minutiae shown in (e) and (f) are manually marked from the original fingerprint.

with original fingerprint and manually marked minutiae, where the level 1 features are extracted at block size 16 pixels. We can see that minutiae extraction from orientation field and ridge frequency field are much more accurate than that from orientation field alone, and the reconstructed fingerprint is very similar to the original fingerprint. The spurious minutiae in the reconstructed fingerprint from orientation field alone are mainly located in regions where ridge frequency varies a lot, for example, in the region close to delta and core points. This is because, in the absence of ridge frequency field, a fixed ridge frequency value was used in reconstructing the fingerprint.

V. Discussion and Conclusions

We have studied the relationship between level 1 (orientation field and ridge frequency field) and level 2 (minutiae set) features and proposed a minutiae detection algorithm given only from level 1 features. The detection is based on the FM model, where a fingerprint can be ideally decomposed into a continuous phase and a spiral phase. The curve integral along a closed path is zero in the continuous phase, but the curve integral along a closed path containing a minutia in the spiral phase is $\pm 2\pi$. Based on these properties, we propose to infer minutiae from the given level 1 features by local curve integral.

It is generally believed that minutiae feature is a type of higher level of fingerprint feature than orientation and ridge frequency. However, our experimental results show that given just the level 1 features, we can recover most of the minutiae. Further, the original fingerprint image can be reconstructed with a high accuracy. We evaluated the reconstructed fingerprints obtained from 1) orientation field and ridge frequency, and from 2) orientation field alone under different block sizes in computing the level 1 features. Both scenarios show the strong correlations between minutiae coordinates and orientation field. The current definition of fingerprint level 1 feature is ambiguity. Based on our results, the level 1 features also contain level 2 features.

The minutiae detection algorithm could be further improved in the following aspects: 1) One possibility to improve the performance is to use an adaptive integral circle. Currently, we are using a circle of fixed radius as the integral path. This may lead to missing minutiae in the circle with opposite polarities because the integral value is zero in this region; 2) For minutiae detection, detecting blobs on the positive and negative minutiae location map separately instead of on the absolute minutiae location map $|P|$ may further improve the performance.

There are still some additional relationships and dependencies among the different fingerprint features that are yet to be discovered. Research on uncovering these relationships

This article has been accepted for publication in a future issue of this journal, but has not been fully edited. Content may change prior to final publication. Citation information: DOI 10.1109/TIFS.2016.2541345, IEEE Transactions on Information Forensics and Security

and dependencies will help us further understand fingerprint models and design more powerful fingerprint recognition systems. In our future work, we will focus on how to remove these dependencies between features in the hope of generating independent feature components of a fingerprint. This will help in synthesizing more realistic fingerprints for creating large fingerprint databases for large scale evaluation.

ACKNOWLEDGMENTS

Eryun Liu's research was partially supported by the National Natural Science Foundation of China under grant No. 61473257 and by the Fundamental Research Funds for the Central Universities. Kai Cao's research was partially supported by the National Natural Science Foundation of China under grant No. 61473214.

REFERENCES

[1] K. G. Larkin and P. A. Fletcher, "A Coherent Framework for Fingerprint Analysis: Are Fingerprints Holograms?" Optics Express, **15**(14), 8667–8677 (2007).
[2] D. Maio and D. Maltoni and R. Cappelli and J. L. Wayman and A. K. Jain, "FVC2002: Second Fingerprint Verification Competition", Proceedings of 16th International Conference on Pattern Recognition, **3**, 811–814, (2002).
[3] A. Ross and J. Shah and A. K. Jain, "From Template to Image: Reconstructing Fingerprints from Minutiae Points", IEEE Transactions on Pattern Analysis and Machine Intelligence, **29**(4), 544–560 (2007).
[4] R. Cappelli and A. Lumini and D. Maio and D. Maltoni, "Fingerprint Image Reconstruction from Standard Templates", IEEE Transactions on Pattern Analysis and Machine Intelligence, **29**(9), 1489–1503 (2007).
[5] J. Feng and A. K. Jain, "Fingerprint Reconstruction: from Minutiae to Phase", IEEE Transactions on Pattern Analysis and Machine Intelligence, **33**(2), 209–223 (2011).
[6] S. Li and A. C. Kot, "An Improved Scheme for Full Fingerprint Reconstruction", IEEE Transactions on Information Forensics and Security, **7**(6), 1906–1912 (2012).
[7] K. Cao and A. K. Jain, "Learning Fingerprint Reconstruction: From Minutiae to Image", IEEE Transactions on Information Forensics and Security, **1**(10), 104–117 (2015).
[8] Wei Tang; Yukun Liu, "Reconstructing ridge frequency map from minutiae template of fingerprints", IEEE Sixth International Conference on Biometrics: Theory, Applications and Systems (BTAS), 2013
[9] David G Lowe, "Distinctive image features from scale-invariant keypoints", International journal of computer vision, **2**(60), 91–110 (2004).
[10] D. C. Ghiglia and M. D. Pritt, "Two-Dimensional Phase Unwrapping: Theory, Algorithms, and Software", Wiley New York, (1998)
[11] H. Bay and A. Ess and T. Tuytelaars and L. Van Gool, "Speeded-up Robust Features (SURF)", Computer Vision and Image Understanding, **110**(3), 346–359 (2008).
[12] NIST Special Database 27, "NIST 8-Bit Gray Scale Images of Fingerprint Image Groups FIGS", http://www.nist.gov/srd/nistsd27.cfm
[13] OpenCV, "Open Source Computer Vision", http://opencv.org
[14] Neurotechnology Inc., "VeriFinger Fingerprint SDK 6.5", http://www.neurotechnology.com, 2013
[15] H. Lin and Y. Wan and A. Jain, "Fingerprint Image Enhancement: Algorithm and Performance Evaluation", IEEE Transactions on Pattern Analysis and Machine Intelligence, **20**(8), 777-789 (1998).
[16] M. Kayaoglu and B. Topcu and U. Uludag, "Standard Fingerprint Databases: Manual Minutiae Labeling and Matcher Performance Analyses", arXiv:1305.1443 [cs.CV], https://www.ekds.gov.tr/bio/databases.html, (2015).
[17] D. Maio, D. Maltoni, R. Cappelli, et al. "FVC2002: Second fingerprint verification competition", Proceedings of the 16th international conference on Pattern recognition, 2002, 3: 811-814.

Eryun Liu received his Bachelor degree in electronic information science and technology from Xidian University, Xi'an, Shaanxi China, in 2006 and Ph.D. degree in Pattern Recognition and Intelligence System from the same university in 2011. He was affiliated with Xidian University as an assistant professor from 2011 to 2013. He was a Post Doctoral Fellow in the Department of Computer Science & Engineering, Michigan State University, East Lansing, USA. He is currently affiliated with the College of Information Science & Electronic Engineering, Zhejiang University, Hangzhou, China, as an assistant professor. His research interests include biometric recognition, point pattern matching and information retrieval, with a focus on fingerprint and palmprint recognition.

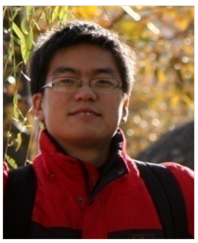

Kai Cao received the Ph.D. degree from the Key Laboratory of Complex Systems and Intelligence Science, Institute of Automation, Chinese Academy of Sciences, Beijing, China, in 2010. He is currently a Post Doctoral Fellow in the Department of Computer Science & Engineering, Michigan State University, East Lansing, USA. He was affiliated with Xidian University as an Associate Professor. His research interests include biometric recognition, image processing and machine learning.